Petrik et al. Highlights and ETOC

Highlights

1) ENaC is high in adult NSCs and neuroblasts
2) Knocking-out ENaC in adult NSCs and neuroblasts decreases their proliferation
3) Fluid flow promotes Na-signals and changes Ca-signals
4) Fluid flow promotes proliferation in ENaC-dependent manner

eTOC

Stem cells need to adapt to signals from environment to regulate their output. Here we show the key role of a flow-sensitive ion channel in regulating the activation of adult neural stem cells and their output.

EPITHELIAL SODIUM CHANNEL REGULATES ADULT NEURAL STEM CELL PROLIFERATION IN A FLOW-DEPENDENT MANNER

David Petrik[1,2], Michael H. Myoga[3,4], Sofia Grade[1,2], Niklas J. Gerkau[5], Melanie Pusch[2], Christine R. Rose[5+], Benedikt Grothe[3,4,6+] and Magdalena Götz[1,2,6,+,*]

[1]Division of Physiological Genomics, Biomedical Center, Ludwig-Maximilians-Universitaet Munich, Planegg-Martinsried, 82152, Germany.

[2]Institute of Stem Cell Research, Helmholtz Center Munich, German Research Center for Environmental Health, Oberschleissheim, 85764, Germany.

[3]Division of Neurobiology, Ludwig-Maximilians-Universitaet Munich, Planegg-Martinsried, 82152, Germany.

[4]Max Planck Institute of Neurobiology, Planegg-Martinsried, 82152, Germany.

[5]Institute of Neurobiology, Faculty of Mathematics and Natural Sciences, Heinrich Heine University Duesseldorf, Duesseldorf 40225, Germany.

[6]SYNERGY, Excellence Cluster of Systems Neurology, Biomedical Center, Ludwig-Maximilians-Universitaet Munich, Germany.

[+]Corresponding authors

*Lead Contact: magdalena.goetz@helmholtz-muenchen.de

SUMMARY

One hallmark of adult neurogenesis is its adaptability to environmental influences. Here we uncovered the epithelial sodium channel (ENaC) as a key regulator of adult neurogenesis as its deletion in neural stem cells (NSCs) and their progeny in the murine subependymal zone (SEZ) strongly impairs their proliferation and neurogenic

output in the olfactory bulb. Importantly, alteration of fluid flow promotes proliferation of SEZ cells in an ENaC-dependent manner eliciting sodium and calcium signals that regulate proliferation via calcium release activated channels and phosphorylation of ERK. Flow-induced calcium signals are restricted to NSCs in contact with the ventricular fluid, thereby providing a highly specific mechanism to regulate NSC behavior at this special interface with the cerebrospinal fluid. Thus, ENaC plays a central role in regulating adult neurogenesis and amongst multiple modes of ENaC function, flow-induced changes in Na signals are critical for NSC biology.

KEYWORDS

Adult neurogenesis, proliferation, neural stem cells, ENaC, fluid flow

INTRODUCTION

Since the discovery of adult neurogenesis in birds and mammals, its regulation by various environmental signals has been a subject of keen interest (Lim and Alvarez-Buylla, 2016). However, adult NSCs in the mammalian brain are located in different niches. In the SEZ, NSCs are embedded in a layer of ependymal cells with their apical ends projecting into the ventricular space filled with cerebrospinal fluid (CSF) (Doetsch et al., 1997; Mirzadeh et al., 2008; Ninkovic and Götz, 2015; Silva-Vargas et al., 2016). This cytoarchitecture places NSCs at the intersection between brain parenchyma and CSF allowing them to sense changes in both and then propagate this information in the syncytium (Lim and Alvarez-Buylla, 2016). Some key elements, such as neuroendocrine peptides and trophic factors (Lehtinen et al., 2011; Silva-Vargas et al., 2016), were identified in the CSF to regulate NSCs biology. Similarly, a gradient of CSF chemorepulsive factors was found to direct migration of

neuroblasts (Sawamoto et al., 2006). However, the molecular sensors detecting the CSF flow remain so far unknown.

Ion channels are prime candidates for such sensor as they can merge different stimuli into a simple and fast signal, the change in flow of ions down the electrochemical gradient and across the plasma membrane. However, NSCs share most electrophysiological properties with astrocytes (Fukuda et al., 2003; Liu et al., 2006), including expression of common voltage-gated potassium channels (Butt and Kalsi, 2006; Pruss et al., 2011). To determine differences in ion channel expression between these cell types, we searched in our previous genome-wide expression analysis and identified the epithelium sodium channel (ENaC) as having higher expression in NSCs compared to parenchymal astrocytes in the diencephalon or cerebral cortex (Beckervordersandforth et al., 2010; Sirko et al., 2015).

ENaC is often located on the apical membrane (Enuka et al., 2012) and controls transepithelial flux of sodium in kidneys or lungs (Hanukoglu and Hanukoglu, 2016), where it is found also in stem cells (Liu et al., 2016). In the nervous system, it is expressed in brain centers controlling fluid volume or blood pressure (Amin et al., 2005), in retina, olfactory bulb (OB) and human cortex (Dyka et al., 2005; Giraldez et al., 2007), in choroid plexus (Van Huysse et al., 2012) and mechanosensory neurons (Fricke et al., 2000). Among glial cells, ENaC has been described in retinal Müller glia (Brockway et al., 2002) and certain glioma cells (Miller and Loewy, 2013).

ENaC is different from other voltage- or ligand-gated channels as it is generally open and hence provides a constant Na-influx. However, its conductance properties and/or opening probability are regulated by many mechanisms including second messengers, proteases and post-translation modifications (Boscardin et al., 2016). Because ENaC is sensitive also to fluid shear stress (Fronius et al., 2010; Wang et al., 2009), it may represent a bona fide candidate for the elusive molecular

sensor detecting CSF flow and linking NSCs with activity of the ciliated ependymal cells that surround them in the SEZ (Mirzadeh et al., 2008).

RESULTS

αENaC is Expressed in NSCs and Progenitors in the SEZ

To determine the localization of ENaC in the SEZ of adult mice, we immuno-stained for the pore-forming alpha subunit of ENaC (αENaC) with cell type-specific antibodies (Figure 1) and observed αENaC in NSCs labeled by the expression of the green fluorescent protein (GFP) driven by the promoter of human glial fibrillary acidic protein (GFAP, Figure 1A) or nestin ((Yamaguchi et al., 2000) Figure S1A) or GFAP- and Sox2-immunoreactivity (Lopez-Juarez et al., 2012), Figure S1B). Indeed, αENaC-staining was also present in the NSCs located in the core of the pinwheel structures (Figure 1B, Figure S1C) labeled by β-catenin and hGFAP-GFP (Beckervordersandforth et al., 2010; Mirzadeh et al., 2008). Also proliferating cells labeled with Ki67 (Scholzen and Gerdes, 2000) and Doublecortin (DCX)+ neuroblasts (Gleeson et al., 1999) were αENaC-immunopositive. Interestingly, this was the case only in the SEZ (Figure 1C,D), and not in the rostral migratory stream (RMS, Figure S1D). Taken together, αENaC was detectable in over 80% of NSCs including proliferating Ki67+GFAP+ NSCs (Figure S1E, F). Also 60% of progenitors and a subset of about 20% neuroblasts (Figure 1E) in the SEZ had detectable levels of αENaC protein. In contrast, niche cells were immunonegative (Figure S1G for oligodendrocyte progenitors, Figure S1H for niche astrocytes), except weak staining in ependymal cells (Figure 1B).

The hippocampal subgranular zone (SGZ) showed more restricted αENaC-immunostaining with rare GFAP+, nestin-GFP+ or Sox2+ NSCs and some DCX+

neuroblasts (Figure S1I-J), while parenchymal astrocytes were ENaC-negative (Figure S1L).

We also checked mRNA levels of α, β and γENaC subunits from dissected SEZ by reverse-transcriptase quantitative polymerase chain reaction (RT-qPCR) and found αENaC expressed much higher than β or γENaC (Figure S1M). The comparison of relative mRNA expression ($2^{-\Delta\Delta Ct}$; (Livak and Schmittgen, 2001) revealed 15 times more αENaC in the SEZ than in the OB, but about 9 times less compared to kidney. When SEZ cells were isolated by fluorescence-activated cell sorting (FACS) as previously described (Codega et al., 2014; Fischer et al., 2011), αENaC but not β or γ expression was detected in quiescent and activated NSCs and ependymal cells (Figure 1F). Neuroblasts had higher αENaC mRNA levels, while virtually nothing was detectable in transiently amplifying progenitors (TAPs) despite the presence of the ENaC protein in these cells (Figure 1C, E). This suggests either fast down-regulation of ENaC mRNA upon dissociation or a high protein stability and inheritance of protein from NSCs in these cells. In order to test if αENaC forms a functional channel in the SEZ, we performed whole-cell patch-clamp recordings and successfully isolated currents sensitive to the ENaC-specific blocker, Benzamil (Alvarez de la Rosa et al., 2013) (Figure 1I-K) in NSCs identified by Aldh1l1-GFP+ (Heintz, 2004) and a radial morphology (Figure 1G,H and S1N).

ENaC is Critical for SEZ Cell Proliferation *In Vitro*

To investigate the functional role of ENaC, we examined neurospheres from adult SEZ (of which 77% cells express αENaC, Figure S2A,B) subjected to genetic knock-down (KD) by esiRNA against αENaC or to pharmacological inhibition by ENaC-specific blockers Benzamil or Amiloride (Alvarez de la Rosa et al., 2013). In proliferating conditions, the αENaC KD, which shows about 60% reduction in ENaC-

immunopositive cells (Figure 2A-C), resulted in significantly fewer cells at 72 hours (h) after transfection (Figure 2D-H). Similarly, incubation of the neurospheres in Amiloride (Figure S2C) or Benzamil (Figure S2D-H) for 24 h significantly reduced the number of cells in a concentration-dependent manner at 72 h after the block. To determine if this reduction in cell number is due to reduced proliferation and/or increased cell death, we followed single cells and their progeny for 85 h by time-lapse imaging of primary SEZ cells as previously described (Ortega et al., 2011). Both αENaC KD (Figure 2I-K) and Benzamil incubation (Figure S2I) significantly decreased the number of divisions and cells generated per individual cell lineage when compared to controls. Moreover, bath application of Benzamil induced rapid cell death (average time 14.2±1.6 h) in about 60% compared to only 6% in control (Figure S2J-L). Thus, reducing function or protein levels of αENaC impairs proliferation and survival of primary SEZ cells. Similarly, SEZ neurosphere-derived cells died as indicated by an increase in TUNEL+ cells upon Amiloride or Benzamil treatment (Figure S2M-O) or KD of αENaC (Figure S2P). Interestingly, αENaC also plays a role in differentiation as KD or blocking of ENaC significantly decreased the proportion of βIII-tubulin+ neurons from primary cells (Figure 2L-N, Figure S2Q-S) or from neurospheres (Figure S3A-F) and also after shorter (6 h) incubation in the ENaC blockers (Figure S3G-I). Noteworthy, pharmacological block by Benzamil showed effects additive to αENaC KD (Figure S2T-X), suggesting either non-specific pharmacological effects or incomplete genetic removal of ENaC. Taken together, limiting ENaC function or protein *in vitro* impairs survival, proliferation and neurogenesis.

Conditional Deletion of αENaC In NSCs *In Vivo* Reduces SEZ Cell Number and Proliferation

Next, we examined the role of αENaC *in vivo* by deleting αENaC selectively in NSCs and their progeny using GLAST^{CreERT2}/CAG-GFP mice (Mori et al., 2006; Nakamura et al., 2006) crossed with Scnn1a$^{flox/flox}$ mice (as gene Scnn1a encodes αENaC; (Hummler et al., 2002) to obtain GLAST^{CreERT2}/CAG-GFP/Scnn1a$^{wt/wt}$ (control) and GLAST^{CreERT2}/CAG-GFP/Scnn1a$^{flox/flox}$ (iENaC) knock-out (KO) mice. Injections of tamoxifen, Tam (Petrik et al., 2012) lead to deletion of Scnn1a and GFP expression in GLAST-expressing cells and their progeny. First, we examined at what time point ENaC protein is lost in the recombined SEZ cells at different times after induction. At 5 days post Tam (DPT) the proportion of αENaC+ cells amongst recombined GFP+ cells was already reduced in iENaC KO, but reached even lower levels by 10 DPT with only about 5% of GFP+ ENaC+ cells left (Figure S4A-C). Therefore, we chose to examine this time-point for a phenotype.

We performed stereological and proportional analyses of GFP+ cells double-stained for Ki67 and DCX at 10DPT (Figure 3A,B). Consistent with the *in vitro* results, the absolute number of GFP+ cells was reduced in the iENaC KO SEZ versus control (Figure 3C). As the reduction in GFP+ cells may be due to a lower recombination rate, we determined the recombination efficiency by assessing the number of recombined GFP+ astrocytes (that are ENaC-negative and hence should not be affected, see Figure S1H) in the cerebral cortex grey matter. The recombined cell numbers at 10 DPT were well comparable in control and iENaC KO cerebral cortex (Figure S4D-F), suggesting a similar level of recombination efficiency between genotypes. Indeed, the decrease in recombined cells resulted in reduced SEZ thickness (measured as the dense band of DAPI+ cells directly adjacent to the lateral ventricle) in iENaC KO compared to controls (Figure 3E). Importantly, these results also indicate that the phenotype in the recombined cells is not compensated by surrounding non-targeted cells.

Next we examined whether GFP+ cells in iENaC KO were reduced by defects in proliferation, survival or fate change. We found fewer proliferating cells (Ki67+GFP+), both progenitors (Ki67+DCX-GFP+) and proliferating neuroblasts (Ki67+DCX+GFP+) in the SEZ of iENaC KO compared to control (Figure 3C), while non-proliferating (Ki67-) neuroblasts were not significantly affected in their number. Likewise, the proportion of progenitors and proliferating and non-proliferating neuroblasts among GFP+ cells showed a significant reduction of all proliferating cells (progenitors and proliferating neuroblasts), while the other populations were relatively less affected in iENaC KO versus control (Figure 3D), emphasizing the effect of ENaC deletion on proliferation.

To determine if NSC numbers are reduced, we discriminated Sox2+ (GFAP-) progenitors and Sox2+GFAP+ NSCs (Figure 3F). Indeed, the NSC number was significantly reduced in the iENaC KO SEZ (Figure 3G), suggesting that both NSCs and their proliferating progeny are affected by αENaC ablation.

To address if the reduction in NSCs may be due to an altered fate, we quantified ependymal cells by S100β staining and their position lining the ventricle (Figure 3H). However, their proportion was similar between control and iENaC KO (Figure 3I), suggesting that the reduction in NSCs is not due to conversion into ependyma (Conover et al., 2000); for label-retaining cell measurements, see below. As staining for activated caspase 3 (Figure S4G and Figure 3J), detecting cells in apoptosis, and for TUNEL (Figure S4H-I), detecting also cells dying by necroptosis and ferroptosis, showed no significant increase in cell death in iENaC KO at both 5 and 10 DPT, the *in vivo* phenotype seems mostly to result from reduced proliferation. Importantly, ENaC deletion also reduced the number of GFP+ neurons in the iENaC KO compared to control olfactory bulb (Figure 3K-M), highlighting its key role in regulating adult neurogenesis.

ENaC Deletion *In Vivo* Affects NSC Activation and Cannot Be Compensated at Later Stages

Next, we examined the SEZ at 30 DPT (Figure 4). As expected, we found a larger number of GFP+ cells in the control SEZ compared to 10 DPT as further progeny has been generated from NSCs (Figure 4A,C). Conversely, in the iENaC KO SEZ there was virtually no increase in GFP+ cell number during these additional 20 days (compare Figures 3C and 4C). Indeed, proliferation was drastically reduced at 30 DPT (Figure 4A-D). To determine if this is due to a depletion of NSCs by cell death and/or proliferation, we provided BrdU, a thymidine analog, in drinking water for two weeks followed by a week of BrdU-free water. Then, Tam was administered and followed by another thymidine analog, EdU, in drinking water for a week. The analysis of GFP+GFAP+ and BrdU+ or EdU+ NSCs was performed at 7 DPT (19 days after BrdU, Figure 4E,F). The proportion of NSCs proliferating after ENaC deletion (EdU+GFAP+GFP+) was significantly reduced in iENaC KO compared to control, whereas the proportion of NSCs proliferating before (BrdU+GFAP+GFP+) was not (Figure 4G). This suggests that ENaC loss leads to reduced proliferation of NSCs, while NSCs that were dividing (and incorporating BrdU) before ENaC loss were not affected. Also, we observed a reduction in proportion of BrdU+GFAP+GFP+ cells in iENaC KO when animals were given BrdU for 2 weeks after Tam and killed one week post BrdU (data not shown), supporting the notion that mostly NSC proliferation is affected by ENaC knock-out, even though we cannot fully rule out cell death or migration out of the niche as contributing to the severe depletion of NSCs. As a consequence of this depletion, the number of newly generated neurons also remains significantly reduced in the OB of iENaC KO compared to control (Figure 4H-

J), demonstrating the long-term severe effects of ENaC deletion on adult neurogenesis.

αENaC is Required in Fast Proliferating SEZ Progenitors *In Vivo* as Revealed by Their Selective Targeting

To discriminate between the effects of ENaC deletion in NSCs and their progeny, we selectively targeted the rapidly proliferating progenitor cells by murine leukemia virus (MLV) based retroviral delivery of NLS-Cre recombinase (Colak et al., 2008) injected into the SEZ of ENaC$^{wt/wt}$/CAG-GFP (WT) and ENaC$^{flox/flox}$/CAG-GFP mice. Already 3 days post injection (dpi) Ki67+ cells were reduced to almost half amongst all GFP+ cells in the SEZ of ENaC$^{flox/flox}$, as compared to WT mice (Figure S5A-C), demonstrating a very fast effect of αENaC loss on progenitor proliferation without affecting the proportion of apoptotic cells (Figure S5D,E). Thus, the iENaC KO phenotype is not exclusively due to the reduction in aNSC numbers but involves direct effects on proliferation of fast progenitors and neuroblasts.

Fluid Flow Induces Proliferation in SEZ in an ENaC-Dependent Manner

ENaC channels are constitutively open, but their opening probability can be further increased by various mechanisms (Boscardin et al., 2016), including fluid flow (Fronius et al., 2010; Wang et al., 2009). To examine the effects of fluid flow, we used SEZ whole-mounts and subjected them to control or elevated artificial cerebrospinal fluid (ACSF) flow (see Methods and discussion for calculations of the shear stress being in the physiological range) for 4 h (Figure 5A), after which the SEZ was stained and the number of Ki67+ and DCX+ cells was quantified (Figure 5B,C). Interestingly, the number of total Ki67+ proliferating cells and proliferating neuroblasts was significantly increased in the SEZ whole-mount exposed to elevated

fluid flow when compared to control (Figure 5D). Thus, increased flow induces a fast proliferation response.

To determine if ENaC contributes to this response, we applied Benzamil that completely abrogated the flow-induced proliferation response (Figure 5D). Application of the high flow paradigm on the genetic mouse models showed an increase in proliferation only in GFP+ cells in controls, but not in iENaC KO (Figure 5E-G), clearly demonstrating that αENaC is required for this response.

To understand possible downstream signaling pathways mediating the proliferative response to the elevated fluid flow via ENaC, we considered the mitogen-activated protein kinases (Bodart, 2010) as prime candidates given their known involvement in SEZ stem cells activation (Ottone et al., 2014) and recent implication as mediators between mechanical stimuli and cell division (Gudipaty et al., 2017). SEZ whole-mounts from WT mice were subjected to control or elevated ACSF flow as described above and stained for the activated (phosphorylated) form of Erk kinase (pErk; Figure 5H-I). High flow increased number of pErk+Ki67+ and pErk+ proliferating neuroblasts (Figure 5J). This increase was reversed in the presence of Benzamil suggesting that elevated fluid flow requires αENaC to activate Erk kinase. Furthermore, there was a smaller proportion and number of pErk+GFP+ cells in SEZ of iENaC KO compared to controls at 5 DPT (Figure S6F-H), underscoring the link between ENaC and downstream activation of the Erk kinase.

ENaC Loss Affects Flow-Induced Changes in Sodium and Calcium Dynamics in NSCs and Progenitors

To test if high flow directly changes intracellular sodium via ENaC, we performed sodium imaging of the SEZ cells. Acute brain slices from control and iENaC KO mice at 21 DPT (Figure 6A,B) were bolus-loaded with the sodium indicator

SBFI-AM. SBFI-loaded cells were alternately excited at 340 and 380 nm and changes in fluorescence emission were measured during baseline and high ACSF flow periods using the ratiometric wide-field microscopy. The ratio of the SBFI fluorescence (340/380 nm) was calculated and normalized to baseline (Figure 6C) as previously done for recording in parenchymal astrocytes (Langer and Rose, 2009). In controls, 35% of cells (28 out of 80) showed increased fluorescence with the increase in fluid flow, whereas this was not the case for any of the 51 cells imaged in iENaC KO. This difference in distribution of responsive cells is statistically significant ($P < 0.0001$, Fisher's exact test). In the control responsive cells, the fluorescence ratio increased by about 2% after the onset of the high flow (Figure 6D), which corresponds to an increase in the intracellular sodium concentration by about 2.2 mM (based on *in situ* calibrations as described earlier (Meier et al., 2006)). Taken together, this data shows that fluid flow induces sodium influx in ENaC-dependent manner.

To further understand how ENaC may convey the information about the fluid flow to the cells, we conducted calcium imaging experiments. Acute brain slices were loaded with the calcium indicator Oregon Green Bapta 1 (OGB1) and calcium oscillations were monitored in baseline flow (Figure 6E) followed by elevated flow and the baseline recovery. In the post-hoc analysis, we evaluated calcium events in GFP+ cells that separated into cell classes by their morphology and anatomical location as NSCs/progenitors, neuroblasts and ependymocytes (Figure 6F). When cells were classified into positive responders (showing higher frequency of calcium oscillations in elevated fluid flow), non-responders (no change in frequency) and negative responders (reduced frequency) we observed a trend towards more negative and non-responders in the GFP+ NSCs/progenitors of iENaC KO compared to controls (Figure 6G,H). Importantly, the GFP+ NSCs/progenitors from control mice

displayed an increase in the frequency of calcium oscillation in response to elevated ACSF flow, a feature that was not observed iENaC KO (Figure 6I). Thus, our data show that cells lacking ENaC do not have the capacity to respond to increased flow by changing Ca signals.

Notably, however, cells from iENaC KO at 10DPT showed higher frequency of Ca signals at baseline ACSF flow when compared with controls (Figure 6G,I). These results suggest that calcium signaling is dysregulated 10 days after loss of ENaC. While this increase in calcium signaling may be counter-intuitive because the absence of sodium inward conductance should promote hyperpolarization and thus attenuate calcium oscillations, the increase in frequency of Ca signals may well be due to secondary changes at 10DPT. Importantly, αENaC involvement in calcium signals was specific to NSCs/progenitors because there was no difference in Ca signals between control and iENaC KO and between baseline and elevated flow in cells classified as ependymocytes (Figure 6J).

Next, we tested if the shear stress specifically affects only cells facing the ventricle or its influence is projected also to cells located deeper in the niche. We loaded SEZ whole-mounts from controls with OGB1 and recorded calcium events in the NSCs at the surface or deep in the tissue (Figure S6A-F). The pool of surface cells (33 total) contained statistically significantly more cells positively responding to high flow than the deeper cells (27 total, $P < 0.0001$, Fisher's exact test, Figure S6G). Indeed, high flow increased the frequency of calcium events only in the surface, but not the deep cells (Figure S6H), suggesting that contact with the ventricle is critical for cellular responsiveness to shear stress.

To identify the possible source of calcium, we exposed SEZ whole-mounts to a specific blocker of the store-operated Ca release activated Ca (CRAC) channels, BTP-2 (YM-58483; (Parekh, 2010)), given the relatively slow nature of the flow

induced Ca-signals. Similar to Benzamil (Figure 5D), BTP-2 also abrogated the flow-induced increase in proliferating cells or neuroblasts in SEZ (Figure 6K-M), suggesting that CRAC channels are a likely source of calcium in this context. Finally, blocking of CRAC channels also abolished the flow-induced increase in the number of proliferating cells and proliferating neuroblasts positive for pErk (Figure 6N) suggesting that the activation of Erk kinase is downstream of CRAC (Chang et al., 2006).

DISCUSSION

αENaC Channel Activity is a Key Regulator of the SEZ Neurogenic Activity

Here, we provide for the first time a role for a voltage- and ligand-independent ion channel in adult neurogenesis. Our results show that αENaC is expressed in NSCs and their progeny in the SEZ, where it is critical for their proliferation. In addition, we suggest that ENaC allows the NSCs to sense fluid flow as one mechanism regulating the neurogenic process.

While ENaC is an essential component of epithelial cells in the peripheral organs (Hanukoglu and Hanukoglu, 2016), this channel has hardly been studied in the brain, let alone in NSCs. Both qPCR and immunohistochemistry showed the predominant expression of the alpha subunit in both the SEZ tissue and in sorted NSCs and neuroblasts, which is the subunit essential for channel function. While ENaC channels have been suggested to exist in different stoichiometry *in vitro* (Anantharam and Palmer, 2007; Staruschenko et al., 2005), only channels containing αENaC, either alone or with other subunits can form functional channels (Canessa et al., 1993; McNicholas and Canessa, 1997). Indeed, ENaC subunits show different expression profiles in cell-dependent context. For example, colonic epithelia or Müller glia express α, but not β or γ ENaC subunits (Asher et al., 1996; Brockway et al.,

2002) similar to our findings in NSCs. Thus, the lack of β or γ ENaC subunits does not preclude ENaC currents. Indeed, we recorded Benzamil-sensitive currents in Aldh1l1-GFP+ cells with radial glia morphology suggesting functional ENaC currents in NSCs. Moreover, we show flow-induced Na-signals only in the presence, but not absence of αENaC in SEZ cells. Our observation that ENaC blockers at high concentrations (Hirsh et al., 2004) were needed to induce proliferation deficits similar to αENaC knock-down *in vitro* is consistent with the native ENaC channels containing only α or β subunits being less sensitive to these blockers (McNicholas and Canessa, 1997). Importantly, however, αENaC is the subunit essential for channel function, which is why we targeted it for deletion here.

αENaC Regulates Proliferation of NSCs and their Progeny

Our *in vitro* and *in vivo* results jointly point towards the conclusion that ENaC predominantly regulates cell proliferation in the SEZ. Blocking or knocking-down ENaC in neurosphere-derived or primary SEZ cells decreases the proliferation as shown by live imaging and immunostaining for Ki67+. Similarly, knocking-out αENaC in NSCs *in vivo* leads to fewer EdU+ NSCs and their progeny in the SEZ. Furthermore, Cre delivered selectively to the rapidly proliferating cells by viral vectors (Colak et al., 2008) revealed that αENaC is also required for proliferation in progenitors and neuroblasts. Thus αENaC acts in a bimodal manner regulating proliferation of both actively dividing NSCs as well as their progeny. So far, only few reports link ENaC activity to cell cycle progression. For example, blocking ENaC had anti-tumor effects (Matthews et al., 2011) and halted the cell cycle in G0/G1 phase (Rooj et al., 2012).

Notably, the effects of blocking or KD of ENaC *in vitro* included also cell death. However, we did not detect any statistically significant change in apoptotic cells at 5

or 10 DPT in iENaC KO and at 3 days post injection of retroviruses or any change in survival of quiescent NSCs labeled by BrdU prior to the ENaC deletion. The fact we did not observe increased cell death in the iENaC KO *in vivo* cannot rule out a possible contribution of cell death to the severe cellular depletion of the SEZ, but the fact that we could detect increased cell death upon ENaC deletion *in vitro*, but not *in vivo* suggests that some elements of the niche environment *in vivo* are helping to keep ENaC KO cells alive.

Fluid Flow Regulates Proliferation via ENaC in the Whole-Mount SEZ

Our findings that fluid flow stimulates cell proliferation in SEZ in an ENaC-dependent manner suggest that ENaC may serve as a sensor of environmental changes. Indeed, this sensory role for ENaC was previously suggested in taste, mechanosensing or circumventricular organs of the brain (Chandrashekar et al., 2010; Miller and Loewy, 2013). The laminar shear stress elicited by fluid flow increases open probability and thus ENaC currents (Althaus et al., 2007; Karpushev et al., 2010), a phenomenon also observed in native tissues such as endothelial cells in blood vessels or tubules in kidney nephrons (Morimoto et al., 2006; Satlin et al., 2001; Wang et al., 2009).

But how does the shear stress applied here compare to the *in vivo* situation? To our knowledge, direct measurements of the shear stress forces in the lateral ventricle are not available, especially not in mice. In humans, various non-invasive clinical studies were conducted to estimate the CSF velocity (Cohen et al., 2009). Near the fluid-solid interface the velocity is estimated at 0.5-1 mm/sec (Siyahhan et al., 2014; Yamada et al., 2013). However, the CSF velocities are much higher in the bulk fluid movement and can reach up to 5-8 cm/sec under the influence of the cardiac and respiratory cycle phase (Battal et al., 2011; Ozturk et al., 2016). In our

preparation, the ACSF velocity exiting the capillary is around 3 cm/sec, which is within the velocity limits mentioned above. This flow velocity with forces previously shown to stimulate ENaC (Althaus et al., 2007) cause an increase in the intracellular sodium concentration in NSCs in control but not iENaC KO SEZ.

Moreover, the effects of increased fluid flow on proliferation are diminished by Benzamil in WT tissue or do not occur in GFP+ cells lacking αENaC. Finally, the elevated fluid flow activates Erk kinase in ENaC-dependent fashion suggesting that it connects fluid flow with proliferation. Thus, our results not only imply for the very first time fluid flow and hence physical forces as a regulator of adult NSCs proliferation in the SEZ, but also identify the channel ENaC as the central mediator. This is important given the expression of various other mechanosensitive channels in NSCs, such as Piezo and TRP channels (Beckervordersandforth et al., 2010; Blumenthal et al., 2014; Codega et al., 2014) and the proposed role of mechanical forces in regulating Drosophila gut stem cells (He et al., 2018) or embryonic neural stem cells *in vitro* (Park et al., 2017).

Why would NSCs and progenitors need to sense fluid flow? One possibility is that sensing fluid flow may serve as an all-or-none mechanism to detect their presence at the surface of the ventricle. Indeed, our calcium imaging experiments from SEZ whole-mounts support this idea as mostly cells at the surface of the ventricle exhibited increased frequency in Ca-signals in response to changes in fluid flow, whereas deeper cells did not. We therefore suggest that SEZ cells utilize the constant fluid drag forces to sense their presence at the ventricle, rather than actually measuring fluid flow speed as do endothelial or kidney cells. Indeed, this is consistent with the concept that radial glial cells contacting the ventricle, but not those deeper in the SEZ, would act as NSCs (Lim and Alvarez-Buylla, 2016).

However, it is important to recognize that ENaC is also regulated by a wide variety of factors other than mechanical forces, such as extracellular proteases and ions or cytoplasmic kinases and links to the cytoskeleton (Boscardin et al., 2016), which may also be involved in its function in the SEZ. Indeed, reducing ENaC protein in conditions with negligible fluid flow, such as *in vitro* preparations, still affects proliferation and viability of NSCs and progenitor cells. We propose that the constitutively open ENaC channel contributes to the increase in membrane potential in proliferating cells (see e.g. review by (Swayne and Wicki-Stordeur, 2012). The NSCs have low resting membrane potential close to the potassium equilibrium potential of around -80 mV (Liu et al., 2006). However, prior to entering the cell cycle the membrane potential becomes more depolarized (Swayne and Wicki-Stordeur, 2012). Importantly, under normal electrochemical gradient for sodium as it is in NSCs, ENaC carries sodium influx into the cell with the capacity to depolarize the membrane (Bigiani and Cuoghi, 2007; Chifflet et al., 2005). Our data therefore suggest that the constant albeit small influx of sodium may contribute to the change in membrane potential required to initiate proliferation.

ENaC Function Bridges Fluid Flow and Calcium Signaling

Besides the up-stream regulators of ENaC function, we also examined down-stream effectors. We have found that ENaC deletion abrogates flow-dependent increase in intracellular sodium and changes calcium signaling in response to increased fluid flow. Likewise, blocking Orai/STIM CRAC channels abrogated the flow-induced increase in cell proliferation and reduced number of cells positive for phosphorylated Erk kinase. The calcium oscillations we recorded in the SEZ were relatively slow (lasting around ten seconds) consistent with time course of release

from calcium sources (Toth et al., 2016) that were observed before in NSCs of the SEZ (Young et al., 2014).

These results propose the following effects downstream of ENaC. ENaC carries sodium influx into the cell, which depolarizes the membrane potential (Bigiani and Cuoghi, 2007; Chifflet et al., 2005) as discussed above. Increased ENaC activity, as during the high flow conditions, thus proportionally increases sodium influx as shown by live imaging and hence leads to further membrane depolarization (Althaus et al., 2007; Wang et al., 2009). This stimulates calcium exchangers and channels that together with inositol tri-phosphate receptors increase the cytoplasmic calcium concentration (Concepcion and Feske, 2017; Justet et al., 2013). Indeed, it has been shown that sodium influx via ENaC can activate dendritic cells in a calcium-dependent manner (Barbaro et al., 2017). The changes in calcium signaling ultimately trigger repetitive emptying of intracellular calcium stores as well as activate CRAC channels (Parekh, 2010) that were found upstream of activation of Erk kinase to regulate cell proliferation (Chang et al., 2008; Chang et al., 2006). Specifically, changes in calcium signaling were able to influence stem cell activity (Deng et al., 2015) with CRAC channels regulating proliferation of neural progenitors from SEZ (Somasundaram et al., 2014). Furthermore, the calcium-dependent PKC-α can regulate Erk activity, which in turn regulates ENaC function (Eaton et al., 2014), providing another layer of complexity between the signaling factors. As pErk was found to both increase (Mustafa et al., 2008) and decrease ENaC function (Eaton et al., 2014), changes in Erk activation with the high flow or in iENaC KO may also be a part of feedback compensations.

ENaC exerts a powerful control on adult neurogenesis with severe reduction in NSC activation and TAP and neuroblast proliferation resulting in much reduced neuronal output in its absence. We therefore propose a key role of this channel in

regulating adult SEZ neurogenesis. This could have medical repercussions since ENaC blockers are used as diuretics to treat certain types of hypertension, can cross the blood brain or CSF barrier (Alvarez de la Rosa et al., 2013) and may hence have potent side effects on neurogenesis (Ernst et al., 2014). Our results emphasize how important it is to understand regulators of adult neurogenesis and highlight the importance of ion-mediated signaling for neural stem and progenitor behavior in the adult brain.

ACKNOWLDEGEMENTS

We are particularly thankful to Edith Hummler for allowing the use of the floxed alpha ENaC mice (Scnn1a/Tm1.1) and to James D. Stockand for providing expression vectors containing cDNA of mouse ENaC subunits. We are also very grateful to Gabriela Jäger, Tatiana Simon-Ebert, Manja Thorwirth and Detlef Franzen for their excellent technical help, and to the viral vector facility of the SFB 870 (TPZ04-funded by DFG). This project was funded in part by the Marie Curie Fellowship (PIIF-GA-2013-628603) to D.P., DFG collaborative research center “SFB 870: Assembly and Function of Neuronal Circuits” to M.G. and B.G., the German Excellence Initiative (Graduate School of Systemic Neurosciences, LMU, & EXC1010 Synergy), the priority program 1757 to M.G. and C.R.R., and the priority program 1738 and the advanced ERC grant “ChroNeuroRepair” to M.G. All authors declare no conflict of interest.

AUTHOR CONTRIBUTIONS

M.G. conceived the project. D.P. and M.G. conceptualized the project. D.P., S.G., M.H.M., B.G. and M.G. designed experiments. D.P. performed all experiments and analyzed all results other than the following. S.G. performed stereotaxic surgeries.

M.P. performed FACS sorting. D.P. and M.H.M. performed experiments and analyzed results for calcium imaging. N.J.G. and C.R.R. performed experiments and analyzed results for sodium imaging. D.P. and M.G. wrote the paper with feedback from the co-authors.

FIGURE LEGENDS

Figure 1. ENaC Expression in Subependymal Zone

(A) Confocal microphotograph of immunostaining for αENaC and hGFAP-GFP in SEZ (lv = lateral ventricle). (B) αENaC staining in β-catenin pinwheel structures of SEZ whole-mounts. (C) Ki67-positive (Ki67+, arrowhead) and Ki67+DCX+ (arrow) cells in SEZ express αENaC. (D) In SEZ, αENaC overlaps with DCX+ cells. (E) Proportional analysis of adult neural stem cells (NSCs), progenitors (Progen.), proliferating neuroblasts (Prolif. NBs), and NBs. in SEZ that are αENaC+. (F) Relative mRNA fold change of αENaC when compared to GAPDH in cDNA from sorted quiescent NSCs (qNSCs; hGFAP-GFP+, CD133+), activated NSCs (aNSCs, hGFAP-GFP+, CD133+, EGFR+), Progen. (hGFAP-GFP-, CD133-, EGFR+), NBs (PSA-NCAM+), and ependymocytes (EC; hGFAP-GFP-, Prominin+). Microphotographs in bright field (G) and fluorescence (H) showing a patch-clamp electrode on a GFP+ cell on the very edge of SEZ. (I) Patch-clamp experimental paradigm. (J) Voltage-command and an example of whole-cell currents elicited by a -90 mV rectangular pulse (40 ms long) before (black) and 6 minutes after Benzamil perfusion (red). (K) Benz-sensitive currents at -90 mV. Scale bars, all 10 μm. Animals were tested at 6-8 weeks of age. N = 4 for proportional analysis, N = 10 for each 4 FACS sorting, N = 3 for patch-clamp recordings. Data are presented as median ± IQR.

Figure 2. Reduced Proliferation and Survival upon Blocking or Knocking-down of ENaC in Primary SEZ or Neurosphere-derived Cells.

Immunostaining for αENaC and DAPI in primary SEZ cultures 48 h after transfection with control esiRNA (A) or αENaC esiRNA (B). Proportion of primary SEZ cells immunopositive for αENaC normalized to control (C). Representative images of neurospheres after transfection with control esiRNA (D,F) or αENaC esiRNA (E,G) at two time points. (H) Schematics of experimental paradigm and dissociated neurosphere cell number quantification 72 h after esiRNA knock-down (KD) of αENaC normalized to control. Example cell division trees from time-lapse imaging in control (I) or αENaC esiRNA (J) during 85 h after transfection. Quantification of the number of cell divisions and cells per division tree in αENaC KD (K). Representative images of primary SEZ cells grown in differentiating conditions stained as indicated after transfection with control (L) or αENaC (M) esiRNA. (N) Quantification of proportion of cells positive for GFAP or βIII-tubulin. Scale bars, 100 μm (D-G) and 20 μm (A-B, L-M). Animals were tested at 6-8 weeks of age. N = 3 for cell cultures. N = 12-16 for lineage trees. * $P < 0.05$; ** $P < 0.01$ Data are presented as median ± IQR or, given the normal distribution, as mean ± SEM (panel K) .

Figure 3. Phenotype of αENaC Knock-out in GLAST-expressing NSCs and Their Progeny in SEZ at 10 Days After Tamoxifen

Representative images of SEZ from control (A) or iENaC KO (B) brains immuno-stained as indicated. In (C), stereological analysis of absolute number of GFP+ cell subpopulations in SEZ: all proliferating cells (Ki67+), proliferating neuroblasts (Ki67+DCX+), progenitors (Ki67+DCX-), and postmitotic neuroblasts (Ki67-DCX+). Proportional analysis of Ki67+ and/or DCX+ cells in the GFP+ cell population in control or iENaC KO (D). (E) Measurements of average SEZ thickness in μm. (F)

Representative image of SEZ stained for GFAP, GFP and Sox2. (G) Quantification of number of Sox2+GFP+ progenitors and Sox2+GFAP+GFP+ NSCs. (H) Representative image of staining for S100β+ and GFP+ ependymal cells in SEZ. (I) Proportion of S100β+GFP+ cells amongst GFP+ cells in control and iENaC KO mice. (J) Number of activated caspase 3 (AC3)-positive cells in both genotypes. Representative images of the olfactory bulb stained as indicated in control (K) or iENaC KO (L). Quantification of number of GFP-positive cells per mm^3 of olfactory bulb tissue (M), lv = lateral ventricle. Scale bars, 50 μm (A-B, K-L) and 20 μm (F, H). Animals were tested at 9-10 weeks of age, N = 4-5. * $P < 0.05$; ** $P < 0.01$ Data are presented as median ± IQR.

Figure 4. Phenotype of αENaC Knock-out in SEZ at 30 Days After Tamoxifen

Representative images of SEZ stained as indicated in control (A) and iENaC KO (B). (C) Stereological quantification of GFP+ cells labeled as in Figure 3C. Proportional analysis of Ki67+ and/or DCX+ GFP-expressing cells in SEZ of control or iENaC KO (D). SEZ stained for GFP, GFAP and BrdU (E) or EdU (F), arrows pointing to triple-positive cells. (G) Schematics of BrdU administration followed by BrdU chase, tamoxifen (Tam), EdU administration and quantification of the proportion of GFP+GFAP+ cells that had also incorporated BrdU or EdU. Olfactory bulb from Control (H) and iENaC KO (I) stained as indicated. (J) Quantification of GFP+ cells in different layers of olfactory bulb cortex as indicated. Note that cell numbers were quantified by stereology, while in Figure 3M the cells were quantified in mm^3 of OB core tissue due to higher density of cells. Scale bars, 50 μm (A-B, H-I), 10 μm (E,G). Animals were tested at 11-13 weeks of age. N = 6-7 for Tam-treated. N = 4-5 for BrdU-treated. * $P < 0.05$; ** $P < 0.01$ Data are presented as median ± IQR.

Figure 5. Effects of Fluid Flow on Cell Proliferation in SEZ

(A) Schematic depicting the experimental design for flow manipulation with SEZ whole-mounts (anatomical directions: P = posterior, D = dorsal, A = anterior, V = ventral). Representative images of en-face SEZ stained as indicated after being subjected to control (B) or high (C) ACSF flow. (D) Quantification of number of Ki67+ and Ki67+DCX+ (Neuroblast) cells per mm^3 of SEZ tissue without or with Benzamil. Representative images of SEZ stained as indicated in iENaC KO mice at 10 DPT with control (E) and high fluid flow (F). Experimental design and cell quantification of proliferating cells and neuroblasts in control and iENaC KO mice under control and high flow (G). Representative images of SEZ stained as indicated (H,I). Quantification of pErk+ cells per mm^3 of SEZ tissue without or with Benzamil (J). Scale bars, 20 μm. Animals were tested at 7-10 weeks of age, N = 3-5. * $P < 0.05$; ** $P < 0.01$ Data are presented as median ± IQR.

Figure 6. Sodium and Calcium Imaging in SEZ Under Different Flow Conditions

(A) Schematic representation of an acute brain slice subjected to ACSF flow. (B) The experimental design for sodium imaging. (C) Representative traces of changes in SBFI fluorescence ratio as a function of time in SBFI-loaded SEZ cells. The red bar indicates exposure to high flow. (D) The change in flow-induced SBFI fluorescence ratio and intracellular sodium concentration in control flow-responsive cells. (E) The experimental design for calcium imaging. (F) Representative still images of the OGB1-loaded cells in SEZ used for the calcium imaging. Stem/progenitor cells (full arrowhead), neuroblasts (empty arrowheads), ependymal cells (arrows) (G). Representative traces of change in fluorescence (ΔF/F) as a function of time in OGB1-loaded SEZ cells from control and iENaC KO at 10 DPT. The red bar indicates exposure to high flow. (H) Number of stem cells/progenitors sorted by their

responsiveness to elevated fluid flow as indicated in the legend in control and iENaC KO. (I) Frequency of calcium events per minute in baseline or high flow in GFP+ stem cells/progenitors of control and iENaC. (J) Frequency of calcium events per minute in ependymocytes. Animals were tested at 9-10 weeks of age, N = 3-4. Representative images of en-face SEZ stained as indicated after being subjected to control (K) or high flow with BTP-2 (L). (M) Quantification of number of Ki67+ and Ki67+DCX+ cells per mm^3 of SEZ tissue. (N) Quantification of number of pErk+ cells per mm^3. Scale bars, 20 μm. Animals were tested at 7-10 weeks of age, N = 3. * $P < 0.05$; ** $P < 0.01$; *** $P < 0.001$. Data are presented as mean ± SEM (panels D, I, J as they are normally distributed) or median ± IQR (panels M, N).

DECLARATION OF INTEREST

Authors declare no competing interests.

REFERENCES

Althaus, M., Bogdan, R., Clauss, W.G., and Fronius, M. (2007). Mechano-sensitivity of epithelial sodium channels (ENaCs): laminar shear stress increases ion channel open probability. FASEB J *21*, 2389-2399.

Alvarez de la Rosa, D., Navarro-Gonzalez, J.F., and Giraldez, T. (2013). ENaC modulators and renal disease. Curr Mol Pharmacol *6*, 35-43.

Amin, M.S., Wang, H.W., Reza, E., Whitman, S.C., Tuana, B.S., and Leenen, F.H. (2005). Distribution of epithelial sodium channels and mineralocorticoid receptors in cardiovascular regulatory centers in rat brain. Am J Physiol Regul Integr Comp Physiol *289*, R1787-1797.

Anantharam, A., and Palmer, L.G. (2007). Determination of epithelial Na+ channel subunit stoichiometry from single-channel conductances. J Gen Physiol *130*, 55-70.

Asher, C., Wald, H., Rossier, B.C., and Garty, H. (1996). Aldosterone-induced increase in the abundance of Na+ channel subunits. Am J Physiol *271*, C605-611.

Barbaro, N.R., Foss, J.D., Kryshtal, D.O., Tsyba, N., Kumaresan, S., Xiao, L., Mernaugh, R.L., Itani, H.A., Loperena, R., Chen, W*., et al.* (2017). Dendritic Cell Amiloride-Sensitive Channels Mediate Sodium-Induced Inflammation and Hypertension. Cell Rep *21*, 1009-1020.

Battal, B., Kocaoglu, M., Bulakbasi, N., Husmen, G., Tuba Sanal, H., and Tayfun, C. (2011). Cerebrospinal fluid flow imaging by using phase-contrast MR technique. Br J Radiol *84*, 758-765.

Beckervordersandforth, R., Tripathi, P., Ninkovic, J., Bayam, E., Lepier, A., Stempfhuber, B., Kirchhoff, F., Hirrlinger, J., Haslinger, A., Lie, D.C*., et al.* (2010). In vivo fate mapping and expression analysis reveals molecular hallmarks of prospectively isolated adult neural stem cells. Cell Stem Cell *7*, 744-758.

Bigiani, A., and Cuoghi, V. (2007). Localization of amiloride-sensitive sodium current and voltage-gated calcium currents in rat fungiform taste cells. J Neurophysiol *98*, 2483-2487.
Blumenthal, N.R., Hermanson, O., Heimrich, B., and Shastri, V.P. (2014). Stochastic nanoroughness modulates neuron-astrocyte interactions and function via mechanosensing cation channels. Proc Natl Acad Sci U S A *111*, 16124-16129.
Bodart, J.F. (2010). Extracellular-regulated kinase-mitogen-activated protein kinase cascade: unsolved issues. J Cell Biochem *109*, 850-857.
Boscardin, E., Alijevic, O., Hummler, E., Frateschi, S., and Kellenberger, S. (2016). The function and regulation of acid-sensing ion channels (ASICs) and the epithelial Na(+) channel (ENaC): IUPHAR Review 19. Br J Pharmacol *173*, 2671-2701.
Brockway, L.M., Zhou, Z.H., Bubien, J.K., Jovov, B., Benos, D.J., and Keyser, K.T. (2002). Rabbit retinal neurons and glia express a variety of ENaC/DEG subunits. Am J Physiol Cell Physiol *283*, C126-134.
Butt, A.M., and Kalsi, A. (2006). Inwardly rectifying potassium channels (Kir) in central nervous system glia: a special role for Kir4.1 in glial functions. J Cell Mol Med *10*, 33-44.
Canessa, C.M., Horisberger, J.D., and Rossier, B.C. (1993). Epithelial sodium channel related to proteins involved in neurodegeneration. Nature *361*, 467-470.
Chandrashekar, J., Kuhn, C., Oka, Y., Yarmolinsky, D.A., Hummler, E., Ryba, N.J., and Zuker, C.S. (2010). The cells and peripheral representation of sodium taste in mice. Nature *464*, 297-301.
Chang, W.C., Di Capite, J., Singaravelu, K., Nelson, C., Halse, V., and Parekh, A.B. (2008). Local Ca2+ influx through Ca2+ release-activated Ca2+ (CRAC) channels stimulates production of an intracellular messenger and an intercellular pro-inflammatory signal. J Biol Chem *283*, 4622-4631.
Chang, W.C., Nelson, C., and Parekh, A.B. (2006). Ca2+ influx through CRAC channels activates cytosolic phospholipase A2, leukotriene C4 secretion, and expression of c-fos through ERK-dependent and -independent pathways in mast cells. FASEB J *20*, 2381-2383.
Chifflet, S., Hernandez, J.A., and Grasso, S. (2005). A possible role for membrane depolarization in epithelial wound healing. Am J Physiol Cell Physiol *288*, C1420-1430.
Codega, P., Silva-Vargas, V., Paul, A., Maldonado-Soto, A.R., Deleo, A.M., Pastrana, E., and Doetsch, F. (2014). Prospective identification and purification of quiescent adult neural stem cells from their in vivo niche. Neuron *82*, 545-559.
Cohen, B., Voorhees, A., Vedel, S., and Wei, T. (2009). Development of a theoretical framework for analyzing cerebrospinal fluid dynamics. Cerebrospinal Fluid Res *6*, 12.
Colak, D., Mori, T., Brill, M.S., Pfeifer, A., Falk, S., Deng, C., Monteiro, R., Mummery, C., Sommer, L., and Gotz, M. (2008). Adult neurogenesis requires Smad4-mediated bone morphogenic protein signaling in stem cells. J Neurosci *28*, 434-446.
Concepcion, A.R., and Feske, S. (2017). Regulation of epithelial ion transport in exocrine glands by store-operated Ca(2+) entry. Cell Calcium *63*, 53-59.
Conover, J.C., Doetsch, F., Garcia-Verdugo, J.M., Gale, N.W., Yancopoulos, G.D., and Alvarez-Buylla, A. (2000). Disruption of Eph/ephrin signaling affects migration and proliferation in the adult subventricular zone. Nat Neurosci *3*, 1091-1097.
Deng, H., Gerencser, A.A., and Jasper, H. (2015). Signal integration by Ca(2+) regulates intestinal stem-cell activity. Nature *528*, 212-217.
Doetsch, F., Garcia-Verdugo, J.M., and Alvarez-Buylla, A. (1997). Cellular composition and three-dimensional organization of the subventricular germinal zone in the adult mammalian brain. J Neurosci *17*, 5046-5061.
Dyka, F.M., May, C.A., and Enz, R. (2005). Subunits of the epithelial sodium channel family are differentially expressed in the retina of mice with ocular hypertension. J Neurochem *94*, 120-128.
Eaton, A.F., Yue, Q., Eaton, D.C., and Bao, H.F. (2014). ENaC activity and expression is decreased in the lungs of protein kinase C-alpha knockout mice. Am J Physiol Lung Cell Mol Physiol *307*, L374-385.
Enuka, Y., Hanukoglu, I., Edelheit, O., Vaknine, H., and Hanukoglu, A. (2012). Epithelial sodium channels (ENaC) are uniformly distributed on motile cilia in the oviduct and the respiratory airways. Histochem Cell Biol *137*, 339-353.

Ernst, A., Alkass, K., Bernard, S., Salehpour, M., Perl, S., Tisdale, J., Possnert, G., Druid, H., and Frisen, J. (2014). Neurogenesis in the striatum of the adult human brain. Cell *156*, 1072-1083.
Fischer, J., Beckervordersandforth, R., Tripathi, P., Steiner-Mezzadri, A., Ninkovic, J., and Gotz, M. (2011). Prospective isolation of adult neural stem cells from the mouse subependymal zone. Nat Protoc *6*, 1981-1989.
Fricke, B., Lints, R., Stewart, G., Drummond, H., Dodt, G., Driscoll, M., and von During, M. (2000). Epithelial Na+ channels and stomatin are expressed in rat trigeminal mechanosensory neurons. Cell Tissue Res *299*, 327-334.
Fronius, M., Bogdan, R., Althaus, M., Morty, R.E., and Clauss, W.G. (2010). Epithelial Na+ channels derived from human lung are activated by shear force. Respir Physiol Neurobiol *170*, 113-119.
Fukuda, S., Kato, F., Tozuka, Y., Yamaguchi, M., Miyamoto, Y., and Hisatsune, T. (2003). Two distinct subpopulations of nestin-positive cells in adult mouse dentate gyrus. J Neurosci *23*, 9357-9366.
Giraldez, T., Afonso-Oramas, D., Cruz-Muros, I., Garcia-Marin, V., Pagel, P., Gonzalez-Hernandez, T., and Alvarez de la Rosa, D. (2007). Cloning and functional expression of a new epithelial sodium channel delta subunit isoform differentially expressed in neurons of the human and monkey telencephalon. J Neurochem *102*, 1304-1315.
Gleeson, J.G., Lin, P.T., Flanagan, L.A., and Walsh, C.A. (1999). Doublecortin is a microtubule-associated protein and is expressed widely by migrating neurons. Neuron *23*, 257-271.
Gudipaty, S.A., Lindblom, J., Loftus, P.D., Redd, M.J., Edes, K., Davey, C.F., Krishnegowda, V., and Rosenblatt, J. (2017). Mechanical stretch triggers rapid epithelial cell division through Piezo1. Nature *543*, 118-121.
Hanukoglu, I., and Hanukoglu, A. (2016). Epithelial sodium channel (ENaC) family: Phylogeny, structure-function, tissue distribution, and associated inherited diseases. Gene *579*, 95-132.
He, L., Si, G., Huang, J., Samuel, A.D.T., and Perrimon, N. (2018). Mechanical regulation of stem-cell differentiation by the stretch-activated Piezo channel. Nature *555*, 103-106.
Heintz, N. (2004). Gene expression nervous system atlas (GENSAT). Nat Neurosci *7*, 483.
Hirsh, A.J., Sabater, J.R., Zamurs, A., Smith, R.T., Paradiso, A.M., Hopkins, S., Abraham, W.M., and Boucher, R.C. (2004). Evaluation of second generation amiloride analogs as therapy for cystic fibrosis lung disease. J Pharmacol Exp Ther *311*, 929-938.
Hummler, E., Merillat, A.M., Rubera, I., Rossier, B.C., and Beermann, F. (2002). Conditional gene targeting of the Scnn1a (alphaENaC) gene locus. Genesis *32*, 169-172.
Justet, C., Evans, F., Vasilskis, E., Hernandez, J.A., and Chifflet, S. (2013). ENaC contribution to epithelial wound healing is independent of the healing mode and of any increased expression in the channel. Cell Tissue Res *353*, 53-64.
Karpushev, A.V., Ilatovskaya, D.V., and Staruschenko, A. (2010). The actin cytoskeleton and small G protein RhoA are not involved in flow-dependent activation of ENaC. BMC Res Notes *3*, 210.
Langer, J., and Rose, C.R. (2009). Synaptically induced sodium signals in hippocampal astrocytes in situ. J Physiol *587*, 5859-5877.
Lehtinen, M.K., Zappaterra, M.W., Chen, X., Yang, Y.J., Hill, A.D., Lun, M., Maynard, T., Gonzalez, D., Kim, S., Ye, P.*, et al.* (2011). The cerebrospinal fluid provides a proliferative niche for neural progenitor cells. Neuron *69*, 893-905.
Lim, D.A., and Alvarez-Buylla, A. (2016). The Adult Ventricular-Subventricular Zone (V-SVZ) and Olfactory Bulb (OB) Neurogenesis. Cold Spring Harb Perspect Biol *8*.
Liu, X., Bolteus, A.J., Balkin, D.M., Henschel, O., and Bordey, A. (2006). GFAP-expressing cells in the postnatal subventricular zone display a unique glial phenotype intermediate between radial glia and astrocytes. Glia *54*, 394-410.
Liu, Y., Jiang, B.J., Zhao, R.Z., and Ji, H.L. (2016). Epithelial Sodium Channels in Pulmonary Epithelial Progenitor and Stem Cells. Int J Biol Sci *12*, 1150-1154.
Livak, K.J., and Schmittgen, T.D. (2001). Analysis of relative gene expression data using real-time quantitative PCR and the 2(-Delta Delta C(T)) Method. Methods *25*, 402-408.

Lopez-Juarez, A., Remaud, S., Hassani, Z., Jolivet, P., Pierre Simons, J., Sontag, T., Yoshikawa, K., Price, J., Morvan-Dubois, G., and Demeneix, B.A. (2012). Thyroid hormone signaling acts as a neurogenic switch by repressing Sox2 in the adult neural stem cell niche. Cell Stem Cell *10*, 531-543.
Matthews, H., Ranson, M., and Kelso, M.J. (2011). Anti-tumour/metastasis effects of the potassium-sparing diuretic amiloride: an orally active anti-cancer drug waiting for its call-of-duty? Int J Cancer *129*, 2051-2061.
McNicholas, C.M., and Canessa, C.M. (1997). Diversity of channels generated by different combinations of epithelial sodium channel subunits. J Gen Physiol *109*, 681-692.
Meier, S.D., Kovalchuk, Y., and Rose, C.R. (2006). Properties of the new fluorescent Na+ indicator CoroNa Green: comparison with SBFI and confocal Na+ imaging. J Neurosci Methods *155*, 251-259.
Miller, R.L., and Loewy, A.D. (2013). ENaC gamma-expressing astrocytes in the circumventricular organs, white matter, and ventral medullary surface: sites for Na+ regulation by glial cells. J Chem Neuroanat *53*, 72-80.
Mirzadeh, Z., Merkle, F.T., Soriano-Navarro, M., Garcia-Verdugo, J.M., and Alvarez-Buylla, A. (2008). Neural stem cells confer unique pinwheel architecture to the ventricular surface in neurogenic regions of the adult brain. Cell Stem Cell *3*, 265-278.
Mori, T., Tanaka, K., Buffo, A., Wurst, W., Kuhn, R., and Gotz, M. (2006). Inducible gene deletion in astroglia and radial glia--a valuable tool for functional and lineage analysis. Glia *54*, 21-34.
Morimoto, T., Liu, W., Woda, C., Carattino, M.D., Wei, Y., Hughey, R.P., Apodaca, G., Satlin, L.M., and Kleyman, T.R. (2006). Mechanism underlying flow stimulation of sodium absorption in the mammalian collecting duct. Am J Physiol Renal Physiol *291*, F663-669.
Mustafa, S.B., Castro, R., Falck, A.J., Petershack, J.A., Henson, B.M., Mendoza, Y.M., Choudary, A., and Seidner, S.R. (2008). Protein kinase A and mitogen-activated protein kinase pathways mediate cAMP induction of alpha-epithelial Na+ channels (alpha-ENaC). J Cell Physiol *215*, 101-110.
Nakamura, T., Colbert, M.C., and Robbins, J. (2006). Neural crest cells retain multipotential characteristics in the developing valves and label the cardiac conduction system. Circ Res *98*, 1547-1554.
Ninkovic, J., and Götz, M. (2015). How to make neurons--thoughts on the molecular logic of neurogenesis in the central nervous system. Cell Tissue Res *359*, 5-16.
Ortega, F., Costa, M.R., Simon-Ebert, T., Schroeder, T., Gotz, M., and Berninger, B. (2011). Using an adherent cell culture of the mouse subependymal zone to study the behavior of adult neural stem cells on a single-cell level. Nat Protoc *6*, 1847-1859.
Ottone, C., Krusche, B., Whitby, A., Clements, M., Quadrato, G., Pitulescu, M.E., Adams, R.H., and Parrinello, S. (2014). Direct cell-cell contact with the vascular niche maintains quiescent neural stem cells. Nat Cell Biol *16*, 1045-1056.
Ozturk, M., Sigirci, A., and Unlu, S. (2016). Evaluation of aqueductal cerebrospinal fluid flow dynamics with phase-contrast cine magnetic resonance imaging in normal pediatric cases. Clin Imaging *40*, 1286-1290.
Parekh, A.B. (2010). Store-operated CRAC channels: function in health and disease. Nat Rev Drug Discov *9*, 399-410.
Park, M.G., Jang, H., Lee, S.H., and Lee, C.J. (2017). Flow Shear Stress Enhances the Proliferative Potential of Cultured Radial Glial Cells Possibly Via an Activation of Mechanosensitive Calcium Channel. Exp Neurobiol *26*, 71-81.
Petrik, D., Jiang, Y., Birnbaum, S.G., Powell, C.M., Kim, M.S., Hsieh, J., and Eisch, A.J. (2012). Functional and mechanistic exploration of an adult neurogenesis-promoting small molecule. FASEB J *26*, 3148-3162.
Pruss, H., Dewes, M., Derst, C., Fernandez-Klett, F., Veh, R.W., and Priller, J. Potassium channel expression in adult murine neural progenitor cells. Neuroscience *180*, 19-29.
Pruss, H., Dewes, M., Derst, C., Fernandez-Klett, F., Veh, R.W., and Priller, J. (2011). Potassium channel expression in adult murine neural progenitor cells. Neuroscience *180*, 19-29.

Rooj, A.K., McNicholas, C.M., Bartoszewski, R., Bebok, Z., Benos, D.J., and Fuller, C.M. (2012). Glioma-specific cation conductance regulates migration and cell cycle progression. J Biol Chem *287*, 4053-4065.
Satlin, L.M., Sheng, S., Woda, C.B., and Kleyman, T.R. (2001). Epithelial Na(+) channels are regulated by flow. Am J Physiol Renal Physiol *280*, F1010-1018.
Sawamoto, K., Wichterle, H., Gonzalez-Perez, O., Cholfin, J.A., Yamada, M., Spassky, N., Murcia, N.S., Garcia-Verdugo, J.M., Marin, O., Rubenstein, J.L.*, et al.* (2006). New neurons follow the flow of cerebrospinal fluid in the adult brain. Science *311*, 629-632.
Scholzen, T., and Gerdes, J. (2000). The Ki-67 protein: from the known and the unknown. J Cell Physiol *182*, 311-322.
Silva-Vargas, V., Maldonado-Soto, A.R., Mizrak, D., Codega, P., and Doetsch, F. (2016). Age-Dependent Niche Signals from the Choroid Plexus Regulate Adult Neural Stem Cells. Cell Stem Cell *19*, 643-652.
Sirko, S., Irmler, M., Gascon, S., Bek, S., Schneider, S., Dimou, L., Obermann, J., De Souza Paiva, D., Poirier, F., Beckers, J.*, et al.* (2015). Astrocyte reactivity after brain injury-: The role of galectins 1 and 3. Glia *63*, 2340-2361.
Siyahhan, B., Knobloch, V., de Zelicourt, D., Asgari, M., Schmid Daners, M., Poulikakos, D., and Kurtcuoglu, V. (2014). Flow induced by ependymal cilia dominates near-wall cerebrospinal fluid dynamics in the lateral ventricles. J R Soc Interface *11*, 20131189.
Somasundaram, A., Shum, A.K., McBride, H.J., Kessler, J.A., Feske, S., Miller, R.J., and Prakriya, M. (2014). Store-operated CRAC channels regulate gene expression and proliferation in neural progenitor cells. J Neurosci *34*, 9107-9123.
Staruschenko, A., Adams, E., Booth, R.E., and Stockand, J.D. (2005). Epithelial Na+ channel subunit stoichiometry. Biophys J *88*, 3966-3975.
Swayne, L.A., and Wicki-Stordeur, L. (2012). Ion channels in postnatal neurogenesis: potential targets for brain repair. Channels (Austin) *6*, 69-74.
Toth, A.B., Shum, A.K., and Prakriya, M. (2016). Regulation of neurogenesis by calcium signaling. Cell Calcium *59*, 124-134.
Van Huysse, J.W., Amin, M.S., Yang, B., and Leenen, F.H. (2012). Salt-induced hypertension in a mouse model of Liddle syndrome is mediated by epithelial sodium channels in the brain. Hypertension *60*, 691-696.
Wang, S., Meng, F., Mohan, S., Champaneri, B., and Gu, Y. (2009). Functional ENaC channels expressed in endothelial cells: a new candidate for mediating shear force. Microcirculation *16*, 276-287.
Yamada, S., Miyazaki, M., Yamashita, Y., Ouyang, C., Yui, M., Nakahashi, M., Shimizu, S., Aoki, I., Morohoshi, Y., and McComb, J.G. (2013). Influence of respiration on cerebrospinal fluid movement using magnetic resonance spin labeling. Fluids Barriers CNS *10*, 36.
Yamaguchi, M., Saito, H., Suzuki, M., and Mori, K. (2000). Visualization of neurogenesis in the central nervous system using nestin promoter-GFP transgenic mice. Neuroreport *11*, 1991-1996.
Young, S.Z., Lafourcade, C.A., Platel, J.C., Lin, T.V., and Bordey, A. (2014). GABAergic striatal neurons project dendrites and axons into the postnatal subventricular zone leading to calcium activity. Front Cell Neurosci *8*, 10.

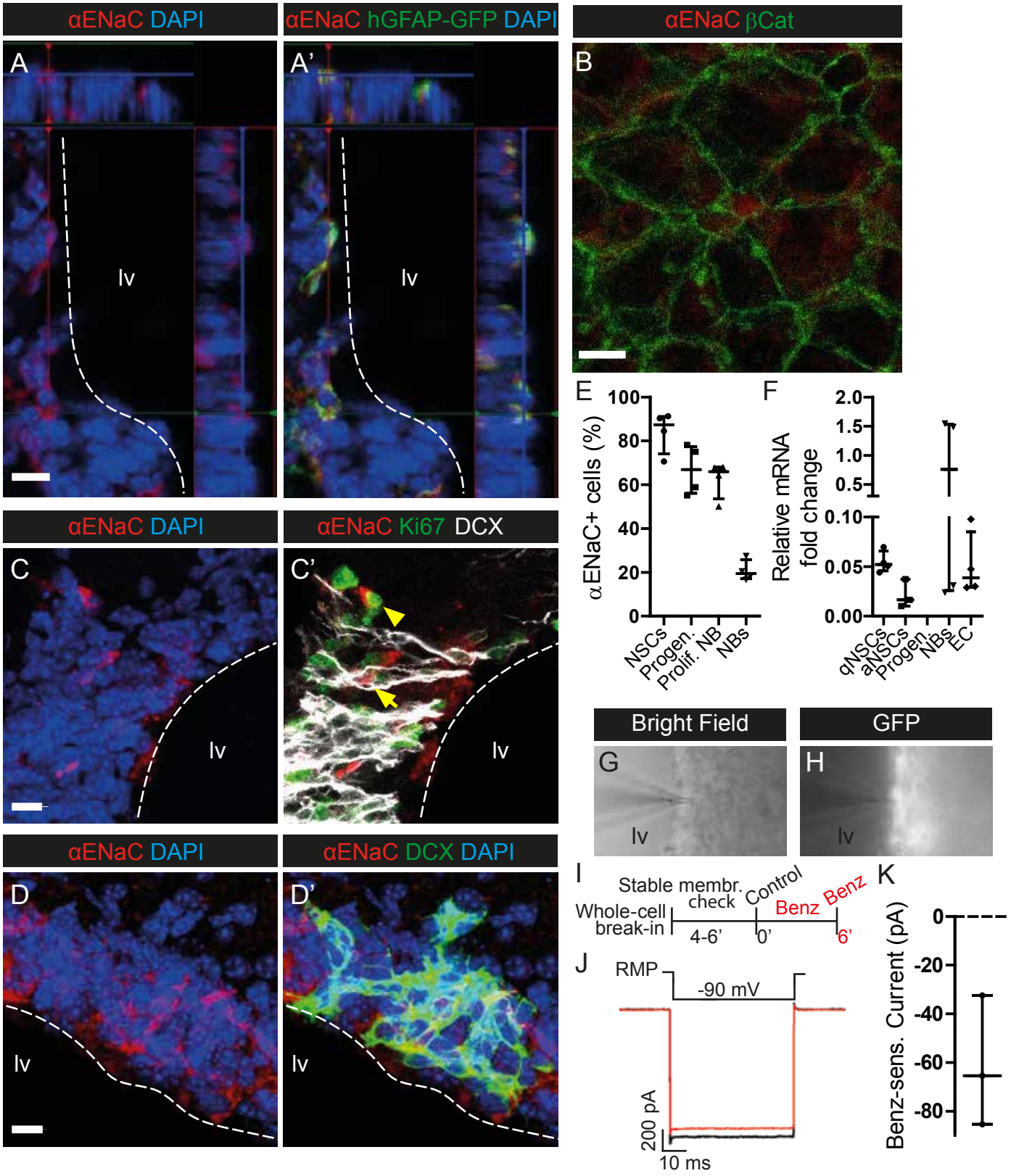
αENaC DAPI
αENaC hGFAP-GFP DAPI
αENaC βCat
A
A'
B
lv
αENaC DAPI
αENaC Ki67 DCX
C
C'
αENaC DAPI
αENaC DCX DAPI
D
D'
E
αENaC+ cells (%)
NSCs
Progen.
Prolif. NB
NBs
F
Relative mRNA fold change
qNSCs
aNSCs
Progen
NBs
EC
Bright Field
GFP
G
H
I
Stable membr. check
Control
Benz
Benz
Whole-cell break-in
4-6'
0'
6'
J
RMP
-90 mV
200 pA
10 ms
K
Benz-sens. Current (pA)

Figure1

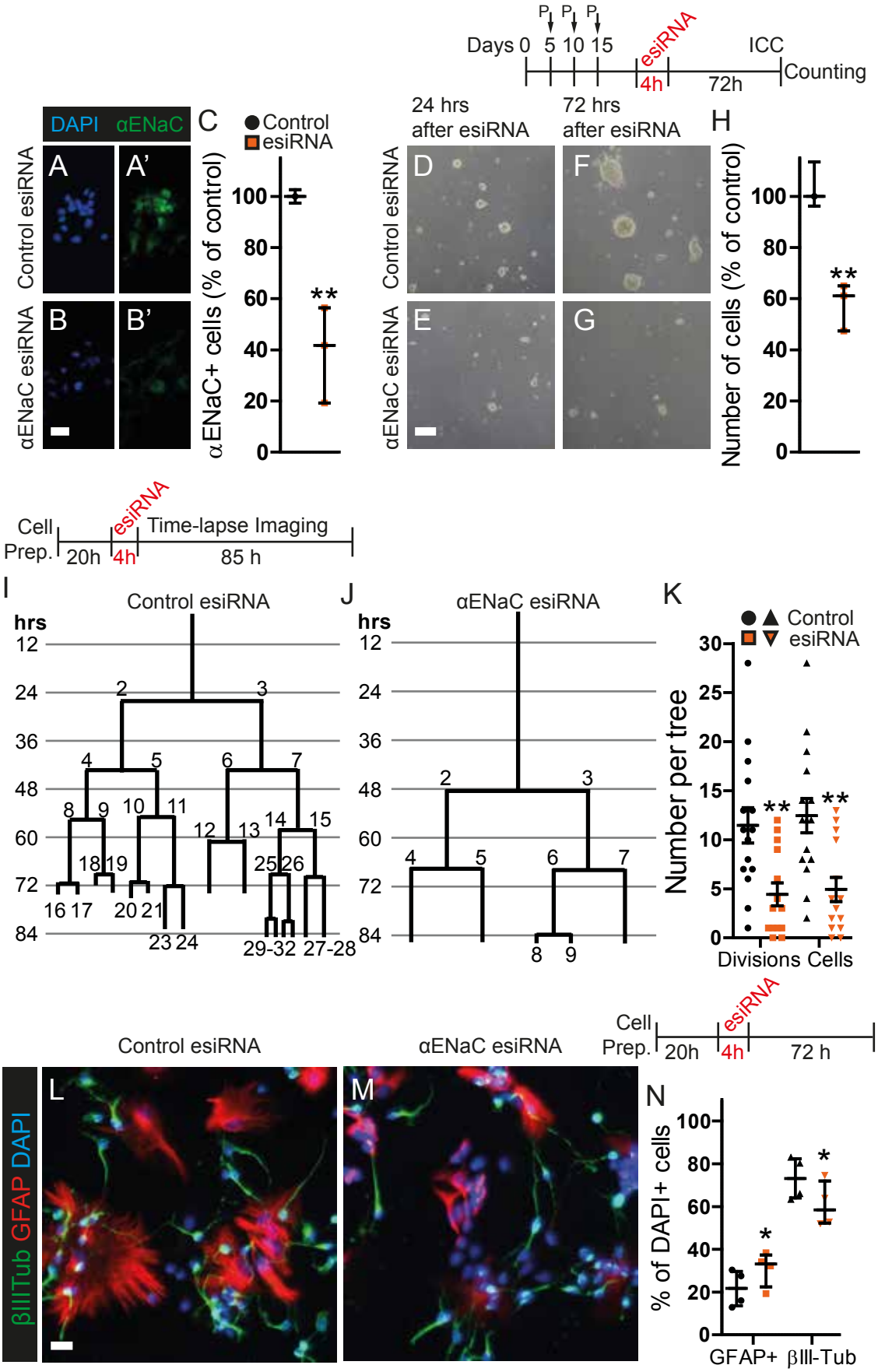
P P P
Days 0 5 10 15
esiRNA
4h
ICC
72h
Counting
DAPI αENaC
Control esiRNA
αENaC esiRNA
A
A'
B
B'
C
Control
esiRNA
αENaC+ cells (% of control)
100
80
60
40
20
0
**
24 hrs after esiRNA
72 hrs after esiRNA
D
F
E
G
H
Number of cells (% of control)
100
80
60
40
20
0
**
Cell Prep.
20h
esiRNA
4h
Time-lapse Imaging
85 h
I
Control esiRNA
hrs
12
24
36
48
60
72
84
2
3
4
5
6
7
8
9
10
11
12
13
14
15
18
19
25
26
16 17
20 21
23 24
29-32
27-28
J
αENaC esiRNA
hrs
12
24
36
48
60
72
84
2
3
4
5
6
7
8
9
K
Control
esiRNA
Number per tree
30
25
20
15
10
5
0
**
**
Divisions
Cells
Control esiRNA
αENaC esiRNA
Cell Prep.
20h
esiRNA
4h
72 h
βIIITub GFAP DAPI
L
M
N
% of DAPI+ cells
100
80
60
40
20
0
*
*
GFAP+
βIII-Tub

Figure2

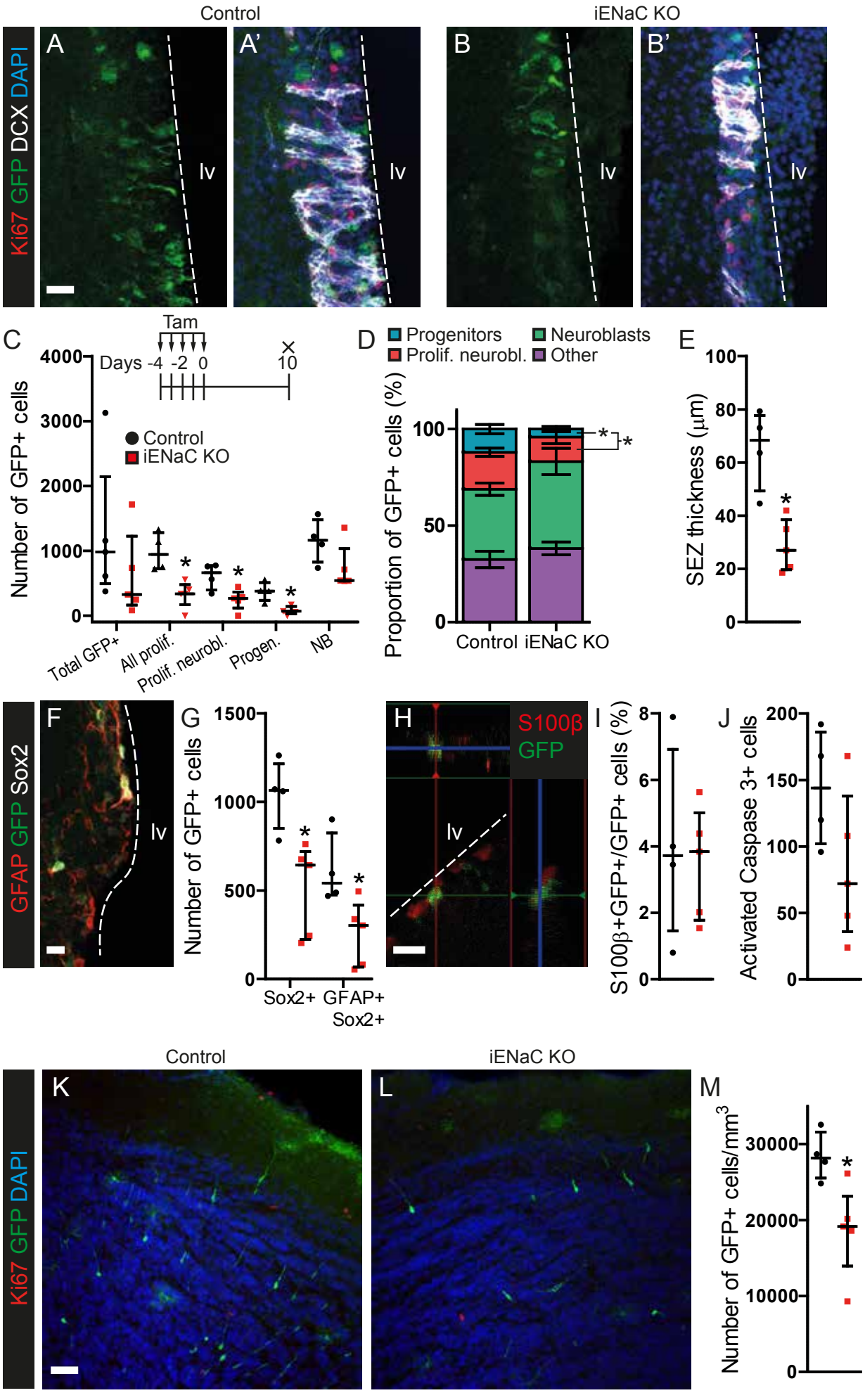
Control
iENaC KO
Ki67 GFP DCX DAPI
A
A'
B
B'
lv
C
Tam
Days -4 -2 0
10
Number of GFP+ cells
Control
iENaC KO
Total GFP+
All prolif.
Prolif. neurobl.
Progen.
NB
D
Progenitors
Neuroblasts
Prolif. neurobl.
Other
Proportion of GFP+ cells (%)
Control iENaC KO
E
SEZ thickness (µm)
GFAP GFP Sox2
F
G
Number of GFP+ cells
Sox2+
GFAP+ Sox2+
H
S100β
GFP
I
S100β+GFP+/GFP+ cells (%)
J
Activated Caspase 3+ cells
Ki67 GFP DAPI
K
L
M
Number of GFP+ cells/mm3

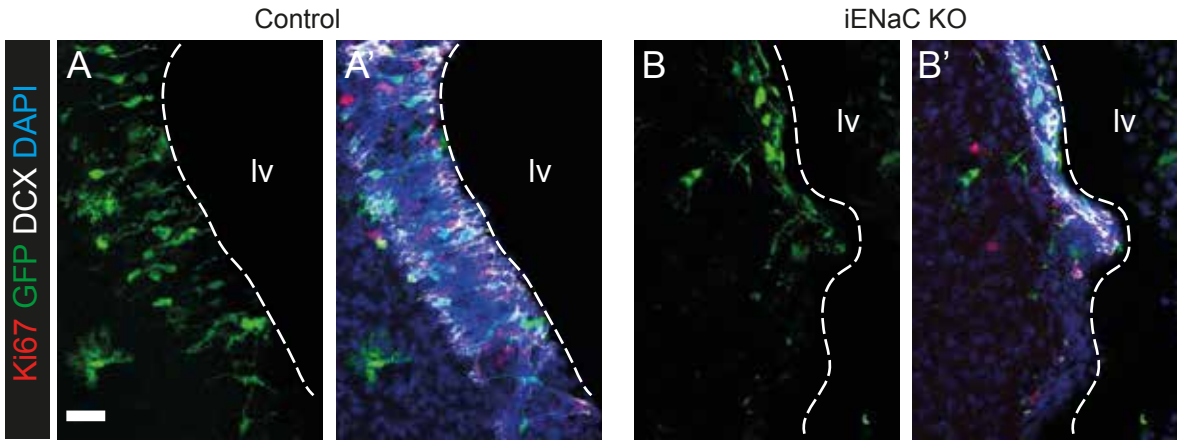
Control
iENaC KO
Ki67 GFP DCX DAPI
A
A'
B
B'
lv

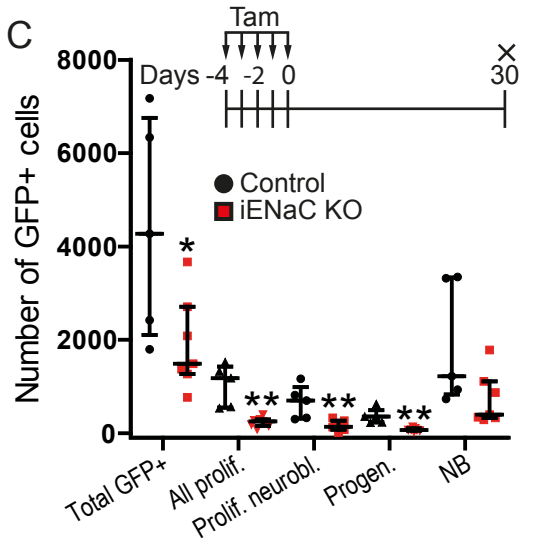
C
Tam
Days -4 -2 0
30
Control
iENaC KO
Number of GFP+ cells
8000
6000
4000
2000
0
Total GFP+
All prolif.
Prolif. neurobl.
Progen.
NB

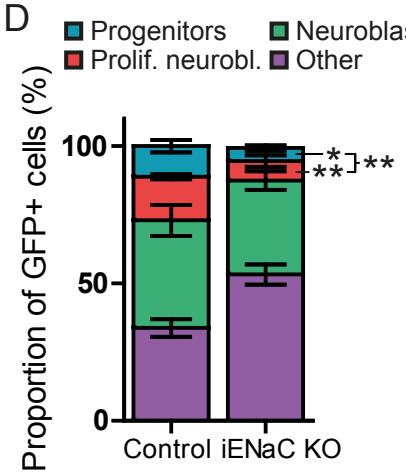
D
Progenitors
Neuroblasts
Prolif. neurobl.
Other
Proportion of GFP+ cells (%)
100
50
0
Control
iENaC KO

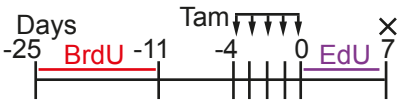
Days
-25
BrdU
-11
Tam
-4
0
EdU
7

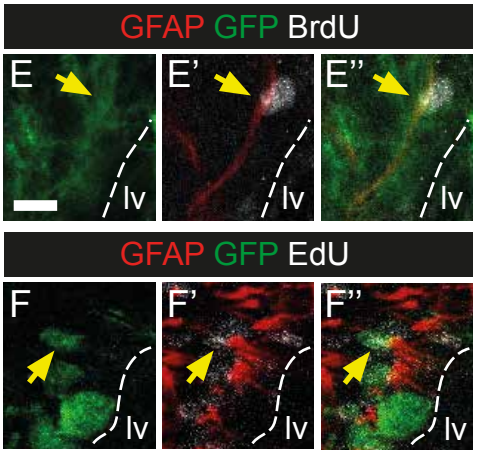
GFAP GFP BrdU
E
E'
E''
lv
GFAP GFP EdU
F
F'
F''

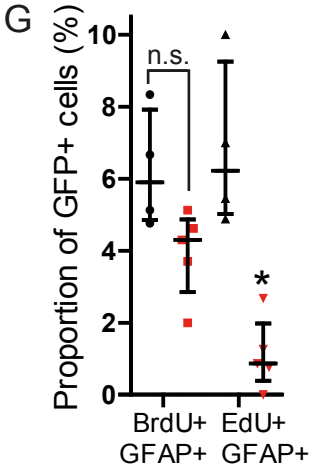
G
Proportion of GFP+ cells (%)
10
8
6
4
2
0
n.s.
BrdU+
GFAP+
EdU+
GFAP+

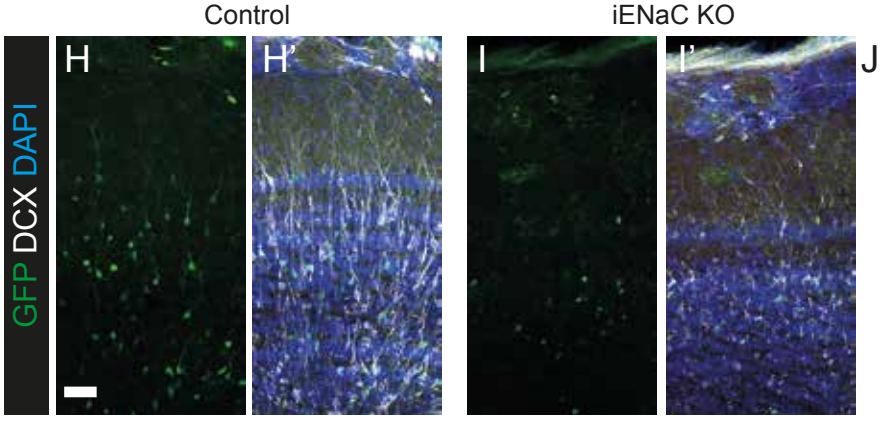
Control
iENaC KO
GFP DCX DAPI
H
H'
I
I'

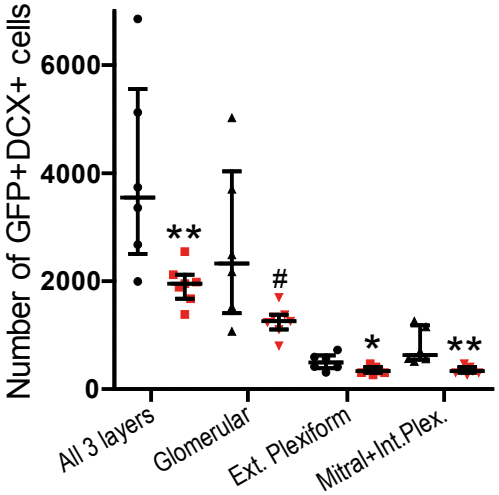
J
Number of GFP+DCX+ cells
6000
4000
2000
0
All 3 layers
Glomerular
Ext. Plexiform
Mitral+Int.Plex.

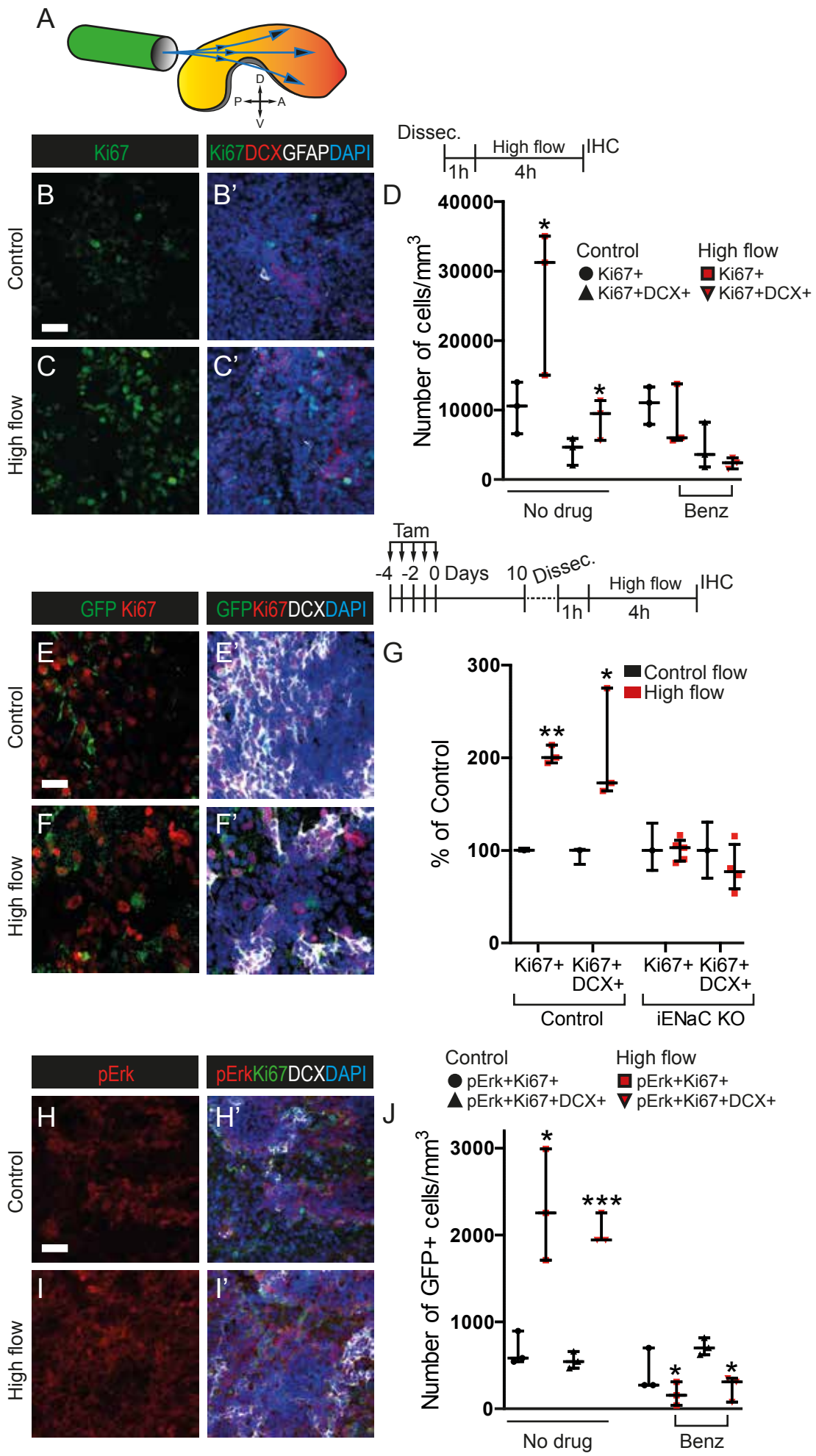
A
D
P
A
V
Ki67
Ki67DCXGFAPDAPI
B
B'
C
C'
Control
High flow
Dissec.
High flow
IHC
1h
4h
D
40000
30000
20000
10000
0
Number of cells/mm3
Control
Ki67+
Ki67+DCX+
High flow
Ki67+
Ki67+DCX+
No drug
Benz
Tam
-4 -2 0 Days
10
Dissec.
High flow
IHC
1h
4h
GFP Ki67
GFPKi67DCXDAPI
E
E'
F
F'
G
300
200
100
0
% of Control
Control flow
High flow
Ki67+
Ki67+ DCX+
Control
iENaC KO
pErk
pErkKi67DCXDAPI
H
H'
I
I'
J
Control
pErk+Ki67+
pErk+Ki67+DCX+
High flow
pErk+Ki67+
pErk+Ki67+DCX+
3000
2000
1000
0
Number of GFP+ cells/mm3
No drug
Benz

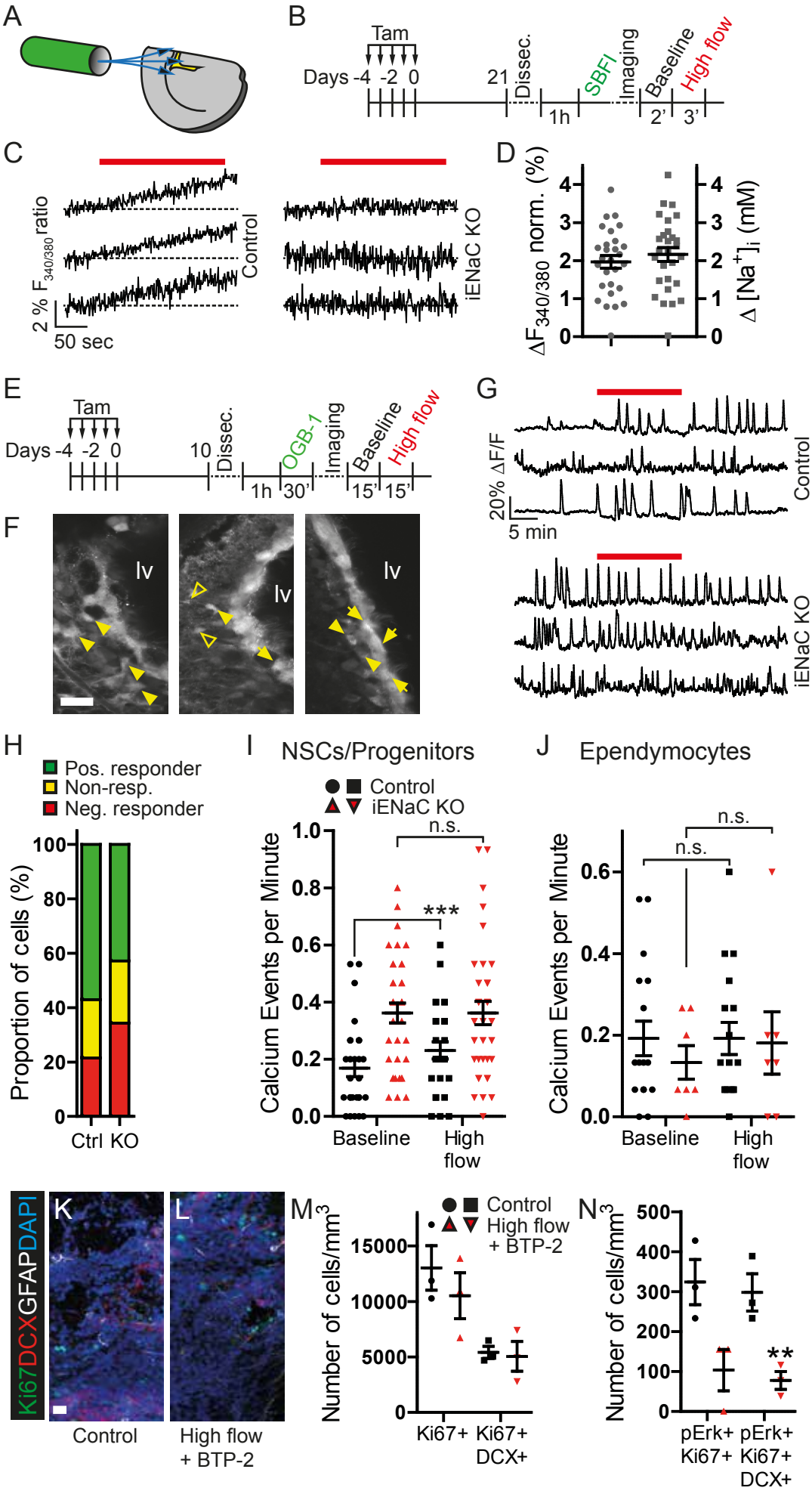
A
B
Tam
Days -4 -2 0
21
Dissec.
1h
SBFI
Imaging
Baseline
2'
High flow
3'
C
2 % F340/380 ratio
50 sec
Control
iENaC KO
D
ΔF340/380 norm. (%)
Δ [Na+]i (mM)
E
Tam
Days -4 -2 0
10
Dissec.
1h
OGB-1
30'
Imaging
Baseline
15'
High flow
15'
F
lv
G
20% ΔF/F
5 min
Control
iENaC KO
H
Pos. responder
Non-resp.
Neg. responder
Proportion of cells (%)
Ctrl
KO
I
NSCs/Progenitors
Control
iENaC KO
n.s.
***
Calcium Events per Minute
Baseline
High flow
J
Ependymocytes
n.s.
n.s.
Calcium Events per Minute
Baseline
High flow
Ki67DCXGFAPDAPI
K
L
Control
High flow
+ BTP-2
M
Control
High flow
+ BTP-2
Number of cells/mm3
Ki67+
Ki67+
DCX+
N
Number of cells/mm3
**
pErk+
Ki67+
pErk+
Ki67+
DCX+